

Uncovering the multifractality of Lagrangian pair dispersion in shock-dominated turbulence

Sadhitro De,^{1,*} Dhruvadya Mitra,^{2,†} and Rahul Pandit^{1,‡}

¹*Department of Physics, Indian Institute of Science, Bangalore 560012, India*

²*Nordita, KTH Royal Institute of Technology and Stockholm University,
Hannes Alfvéns väg 12, 10691 Stockholm, Sweden*

Lagrangian pair dispersion provides insights into mixing in turbulent flows. By direct numerical simulations (DNS) we show that the statistics of pair dispersion in the randomly forced two-dimensional Burgers equation, which is a typical model of shock-dominated turbulence, is very different from its incompressible counterpart because Lagrangian particles get trapped in shocks. We develop a heuristic theoretical framework that accounts for this — a generalization of the multifractal model — whose prediction of the scaling of Lagrangian exit times agrees well with our DNS.

The statistics of the relative pair dispersion of Lagrangian particles (tracers) in turbulent flows has numerous physical applications [1–9]. *Richardson’s law*, a pioneering work in this field, states that, in a turbulent fluid, the mean-squared displacement between a pair of tracers, $\langle R^2(t) \rangle$, at time t , scales as $\langle R^2(t) \rangle \sim t^3$ [10]. In other words, there is a dynamic exponent $z = 3/2$. Richardson’s law can be viewed as a consequence of Kolmogorov’s 1941 (K41) scaling theory of turbulence [see, e.g., Ref. 9]. It is now well established that the K41 theory is incomplete because it does not account for intermittency, which arises predominantly because of the most dissipative structures in the flow and leads to multifractality [11]. In brief, intermittency and multifractality in homogeneous and isotropic turbulence is characterised by the non-trivial scaling properties of moments of velocity differences, $\langle \delta v(\ell)^p \rangle$, over length scales, ℓ , i.e., $\langle \delta v(\ell)^p \rangle \sim \ell^{\zeta_p}$, with the multiscaling exponent ζ_p a nonlinear function of p (K41 yields simple scaling with $\zeta_p = p/3$) [12]. Therefore, it is natural to hypothesize that Richardson’s law must have multiscaling corrections too. In particular, we expect *dynamic multiscaling* [13–17], characterised by not one but an infinity of dynamic exponents; specifically, different moments of $R(t)$ should scale with different powers of t . However, even the most recent experimental [18–22] and numerical [20, 23–27] measurements of $\langle R^2 \rangle$ provide only limited support to Richardson’s law, because the power-law behavior is observed over a range of scales that covers a decade or so. Hence, there seems to be little hope of extracting the dynamic-multiscaling behavior from experimental or numerical measurements of moments of $R(t)$.

It turns out that the *Lagrangian exit time*, conventionally defined as the time taken for the separation between a pair of tracers (Lagrangian interval) to exceed a given threshold (e.g., the *doubling time*) [28–31], provides a robust measure for dynamic multiscaling. From the statistics of these exit times it is possible to extract dynamic

multiscaling exponents that match the predictions from the multifractal model of turbulence [32–34].

We have, so far, outlined Lagrangian pair dispersion in *incompressible* turbulence. We turn now to *shock-dominated turbulence*, which refers to highly *compressible* turbulence wherein the total energy in the irrotational modes is significantly larger than that in the solenoidal modes [35]; this poses formidable challenges that we must confront because such flows are widely prevalent in many astrophysical systems [36]. Over the last two decades, several groups have studied the multifractal properties of compressible turbulence, ranging from flows that are weakly compressible to those that are shock-dominated [37–44]. Additionally, the dynamics of tracers and heavy inertial particles in such systems have also been investigated [45–49]. However, the possible multifractal generalization of Richardson’s law and exit time statistics to compressible turbulence has not been established yet.

We develop the theoretical framework that is required for this generalization to shock-dominated turbulence. It rests on the crucial observation that tracers strongly cluster at the shocks, which comprise the most dissipative structures, making Lagrangian pair dispersion in such flows qualitatively different from that in incompressible turbulence. Consequently, we define two exit times – (i) the *doubling time* and the (ii) *halving time* – as the times taken for a Lagrangian interval to (a) go beyond twice and (b) shrink below half its initial length, respectively. We carry out explicit direct numerical simulations (DNSs) of a simplified model of shock-dominated turbulence, namely, the randomly-forced two-dimensional (2D) Burgers equation, which is not only rich enough to display the complexities of such turbulence [37, 50, 51], but also simple enough for us to develop a heuristic theory for our DNS results. We find that the statistics of the doubling times agree with those that follow from the conventional application of the multifractal model, but those of halving times do not. We generalize this framework to account for the clustering of tracers on shocks and obtain therefrom the scaling exponents for the moments of the distribution of halving times. The results from our

* sadhitrode@iisc.ac.in

† dhruva.mitra@gmail.com

‡ rahul@iisc.ac.in

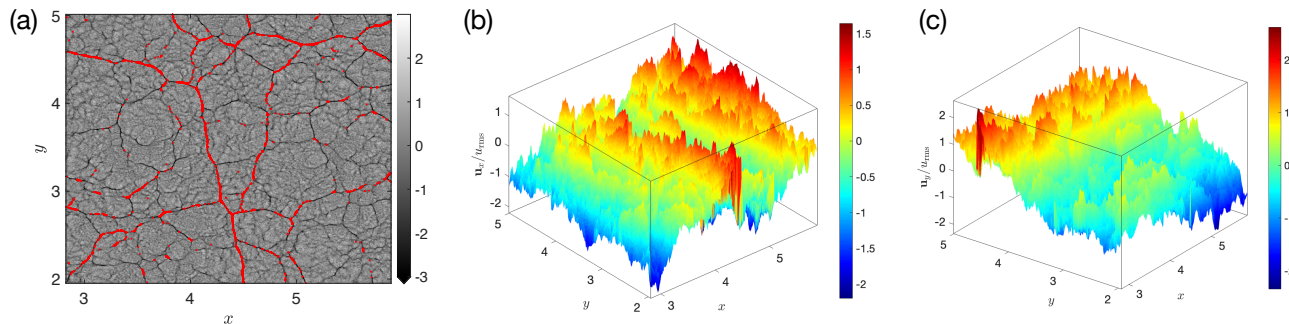


FIG. 1. **Typical snapshots** of a part of our domain in the non-equilibrium statistically steady state of turbulence. (a) The divergence of the velocity field, $\nabla \cdot \mathbf{u}$; shocks are the dark filament-like structures with large negative divergences; instantaneous tracer positions are marked by red dots. The tracers cluster on the shocks. Surface plots of (b) the x -component and (c) the y -component of the velocity field $\mathbf{u}(\mathbf{x}, t)$. The shocks are the large negative jumps.

heuristic theory are in excellent agreement with those from our DNS. In a similar vein, we define and investigate the scaling properties of doubling and halving frequencies of Lagrangian intervals, and try to understand them on the basis of the underlying flow intermittency.

The randomly-forced 2D Burgers equation is:

$$\begin{aligned} \partial_t \mathbf{u} + \mathbf{u} \cdot \nabla \mathbf{u} &= \nu \nabla^2 \mathbf{u} + \mathbf{f}(\mathbf{x}, t); \quad \nabla \times \mathbf{u} = 0; \\ \langle \hat{\mathbf{f}}(\mathbf{k}, t) \cdot \hat{\mathbf{f}}(\mathbf{k}', t') \rangle &\sim |\mathbf{k}|^{-2} \delta(\mathbf{k} + \mathbf{k}') \delta(t - t'). \end{aligned} \quad (1)$$

$\mathbf{u}(\mathbf{x}, t)$ is the Eulerian velocity at position \mathbf{x} and time t , and ν is the coefficient of viscosity. $\mathbf{f}(\mathbf{x}, t)$ is a zero-mean, irrotational, Gaussian, white-in-time random force whose Fourier components $\hat{\mathbf{f}}(\mathbf{k}, t)$ [with \mathbf{k} the wave vector] obey the constraint given in (1). The equal-time and dynamic-scaling properties of the Burgers equation, which can be mapped to the KPZ equation [52], have been studied extensively, but, most often, in one dimension (1D) through DNSs and renormalization-group methods [53–65]. We perform high-resolution pseudo-spectral DNSs of (1) on a bi-periodic square domain with side $L = 2\pi$. After the DNS reaches a non-equilibrium-statistically-stationary state (NESS), we calculate the energy spectrum $E(k)$, which shows a power-law regime that is consistent with $E(k) \sim k^{-5/3}$, over approximately one-and-a-half decades [see Appendix A]. We also calculate the equal-time, longitudinal structure functions S_p and their scaling exponents ζ_p :

$$S_p(r) \equiv \langle |\delta u_{\parallel}(\mathbf{r})|^p \rangle \sim r^{\zeta_p}, \quad (2a)$$

$$\text{where } \delta u_{\parallel}(\mathbf{r}) \equiv [\mathbf{u}(\mathbf{x} + \mathbf{r}) - \mathbf{u}(\mathbf{x})] \cdot \left(\frac{\mathbf{r}}{r}\right). \quad (2b)$$

Here the symbol $\langle \cdot \rangle$ denotes averaging over the NESS. Equation (1) exhibits bi-scaling, given the type of forcing we use [60, 66], i.e., the scaling exponents

$$\zeta_p = \begin{cases} p/3 & \text{for } p < 3, \\ 1 & \text{for } p \geq 3. \end{cases} \quad (3)$$

Our DNS results largely agree with this [67]. In the NESS, we seed the flow uniformly with tracers and track

their subsequent motion. We present a pseudo-gray-scale plot of $\nabla \cdot \mathbf{u}$ in Fig. (1a), in which shocks are visible as dark filamentary structures. Tracers, shown in red, accumulate on these shocks. In Fig. (1b) and Fig. (1c) we give, respectively, illustrative surface plots of the x - and y -components of $\mathbf{u}(\mathbf{x}, t)$ at the same instant of time as for Fig. (1a). In these surface plots, the shocks appear as large negative jumps. Henceforth, we non-dimensionalize all quantities by using L and $T_L \equiv \mathcal{L}_I/u_{\text{rms}}$, the large-eddy-turnover time, with u_{rms} the root-mean-square velocity and \mathcal{L}_I the integral length scale [see Appendix A for details].

For a Lagrangian interval of initial length R_0 , within the inertial range, a naive application of the multifractal model of turbulence, as done previously [28–30], yields the following scaling exponents of the order- p moments of the doubling times, τ_D :

$$\langle \tau_D^p(R_0) \rangle \sim R_0^{\kappa_p^D}, \quad (4a)$$

$$\text{where } \kappa_p^D = \zeta_{-p} + p. \quad (4b)$$

The second of these equations gives the bridge relation between the dynamic exponent, κ_p^D , and the equal-time exponent, ζ_{-p} . We probe the validity of this bridge relation only for $p < 1$, because the structure functions of negative order, $S_{-p}(r)$, exist only in this regime [68, 69]. We calculate κ_p^D and ζ_{-p} , from our DNS and plot them versus p in Fig. 2. Clearly (4b) holds within error bars. By construction, the multifractal model does not distinguish between the scaling behaviors of doubling times and halving times, τ_H . This may lead us to expect, for compressible turbulence, that the moments of τ_H should have the same scaling as the moments of τ_D , i.e., $\langle \tau_H^p(R_0) \rangle \sim R_0^{\kappa_p^H}$ with $\kappa_p^H = \kappa_p^D$. Our DNS, see Fig. (2), shows that this *naive expectation is false*, because $\kappa_p^D \neq \kappa_p^H$.

We must, therefore, generalize the multifractal model in order to construct a theory that yields the p -dependence of κ_p^H shown in Fig. (2). We first outline the standard argument that is used to understand Richardson's law [9]. A Lagrangian interval of length, $R(t)$, un-

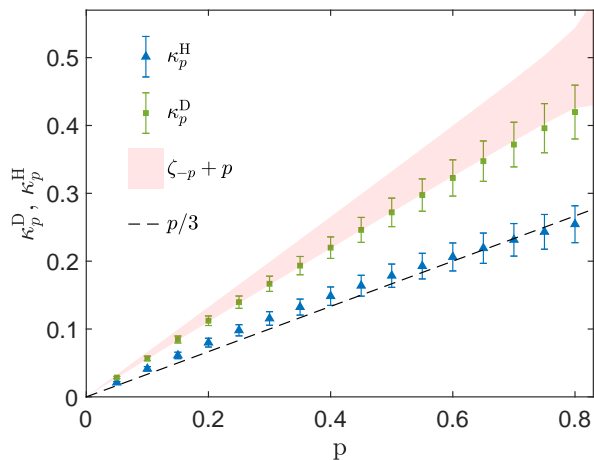


FIG. 2. **Dynamic scaling exponents**, of order p , as a function of p for the doubling times κ_p^D (triangles) and halving times κ_p^H (squares) of Lagrangian intervals. Clearly, contrary to the naive expectation based on the conventional multifractal model, $\kappa_p^D \neq \kappa_p^H$. The region shaded in light pink is the multifractal prediction (4), where the equal-time scaling exponents ζ_{-p} and their error bars are calculated from our DNS. The dashed line is our theoretical prediction (8), which agrees very well with the numerical results.

dergoes a Brownian motion (we restrict ourselves to 2D) with a diffusivity, $K(R)$, that depends on R itself, i.e., the probability distribution function (PDF) of R , namely, $W(R, t)$, satisfies

$$\partial_t W = \frac{1}{R} \partial_R [R K(R) \partial_R W]. \quad (5)$$

The R -dependence of $K(R)$ is deduced from the following dimensional arguments: $K \sim (\delta_R V)^2 t_{\text{cor}}$, where $\delta_R V$ is the typical velocity difference across the scale, R , and t_{cor} is the typical correlation time. If we now use the K41 forms, $\delta_R V \sim R^{1/3}$ and $t_{\text{cor}} \sim R/\delta_R V \sim R^{2/3}$, we get $K \sim R^{4/3}$ which, when substituted in (5), yields Richardson's law [70].

To carry out a similar calculation for 2D Burgers turbulence, we need an appropriate scaling form of $K(R)$. The first, straightforward, generalization is to replace the K41 result, $\delta_R V \sim R^{1/3}$, with $\delta_R V \sim R^h$, where h is the scaling exponent of the velocity field. The second key idea is to recognize that, when we consider a Lagrangian interval of length R here, we must distinguish between the following three possibilities for this interval:

1. Case (1) [interval along a shock]: $\delta_R V \sim R^h$, but the typical correlation time is determined by sweeping as both ends of the interval are trapped in the same shock, so $t_{\text{cor}} \sim R$, whence $K \sim R^{2h+1}$.
2. Case (2) [interval straddles a shock]: $\delta_R V$ is a constant, independent of R , i.e., $h = 0$, and $t_{\text{cor}} \sim R$, consequently $K \sim R$.
3. Case (3) [interval is away from shocks]: The interval can decrease in only one of the following two ways:

- (A) Case (3A): Both ends of the interval get trapped, at a later time, in the same shock, so the arguments used in case (1) apply. Therefore, at late times, $K \sim R^{2h+1}$.
- (B) Case (3B): The two ends of the interval get trapped in two different shocks, which then approach each other. Hence, $\delta_R V$ is then the velocity difference between the two shocks, which does not depend on R . Since $t_{\text{cor}} \sim R$, this yields $K \sim R$ at late times.

In all of these cases, the calculation of the PDF of halving times is a first-passage problem for (5), with two boundaries, one at $R \rightarrow \infty$ and the other at $R = R_0/2$, where $R_0 \equiv R(t = 0)$. Given the forms of $K(R)$ in Cases (1)-(3), it is sufficient to calculate the halving time PDFs, \mathcal{P}_1 and \mathcal{P}_2 , for $K \sim R^{2h+1}$ and $K \sim R$, respectively. We obtain [71]

$$\mathcal{P}_1(\tau_H, R_0) \sim \frac{1}{R_0^{1-2h}} \exp \left[-A_1 \frac{\tau_H}{R_0^{1-2h}} \right] \quad \text{and} \quad (6a)$$

$$\mathcal{P}_2(\tau_H, R_0) \sim \frac{1}{R_0} \exp \left[-A_2 \frac{\tau_H}{R_0} \right], \quad (6b)$$

where A_1 and A_2 are numerical constants [see Appendix B for details]. By collecting all the cases together, we find the overall PDF of τ_H , for large τ_H :

$$\mathcal{P}(\tau_H, R_0) \sim w_1 \mathcal{P}_1 + w_2 \mathcal{P}_2 + w_{3A} \mathcal{P}_1 + w_{3B} \mathcal{P}_2, \quad (7)$$

where w_1 , w_2 , w_{3A} , and w_{3B} are the relative weights for the Cases discussed above. As the shocks are one-dimensional structures, w_1 is negligible, but the other weights are not; and in the limit $R_0 \rightarrow 0$, $w_{3A} \mathcal{P}_1$ is the dominant contribution. Thereby, we obtain the following result for the moments of the PDF of τ_H :

$$\langle \tau_H^p \rangle \sim R_0^{p(1-2h)} \sim R_0^{p/3}. \quad (8)$$

In the final step we substitute $h = 1/3$ [60, 66]. Equation 8 agrees well with our numerical results [see the dashed line in Fig. (2)].

Several important comments are now in order:

- (a) We emphasize that, although the halving-time dynamic exponent κ_p^H depends linearly on the order p , the statistics of halving times is *not Gaussian* – the tail of the PDF of τ_H is exponential [see (6) and (7)]. Furthermore, (8) *does not* imply simple dynamic scaling because we have shown explicitly that differently defined time-scales have different scaling exponents.
- (b) Although we discuss halving and doubling times, explicitly, our results apply to exit times in general.
- (c) Even though our DNS study is limited to the randomly-forced 2D Burgers equation 1, our theoretical arguments can be generalized to other, richer varieties of shock-dominated turbulence in a straightforward manner, as long as the equal-time scaling exponents, ζ_p , are known.

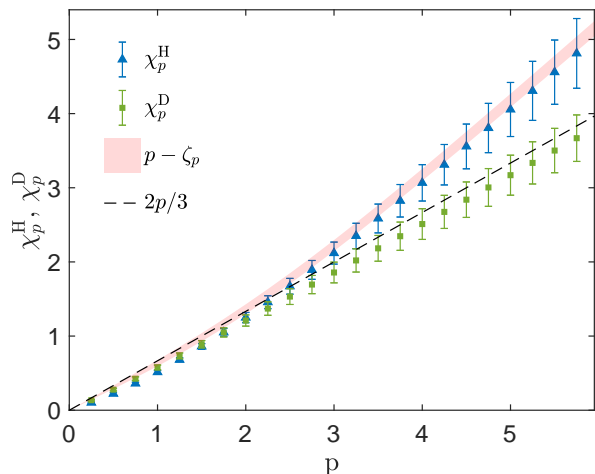


FIG. 3. **Dynamic scaling exponents**, of order p as a function of p for the doubling frequencies χ_p^D (squares) and halving frequencies χ_p^H (triangles) of Lagrangian intervals. Clearly, contrary to the naive expectation based on the conventional multifractal model, $\chi_p^D \neq \chi_p^H$ for all p . The region shaded in light pink is the predicted bridge relation $\chi_p^H = p - \zeta_p$, where the equal-time scaling exponents ζ_p and their error bars are calculated from our DNS. The dashed line is our prediction for χ_p^D .

A critical problem with the multifractal description of the scaling of exit times is that the bridge relation 4, requires the calculation of negative moments of $\delta_R V$. One way to avoid the calculation of such moments is to consider the statistics of *inverse* exit times. In particular, we define the halving and doubling frequencies to be $\omega_H \equiv 1/\tau_H$ and $\omega_D \equiv 1/\tau_D$, respectively. Thereby we define two new sets of dynamic scaling exponents,

$$\langle \omega_H^p(R_0) \rangle \sim R_0^{-\chi_p^H} \quad \text{and} \quad \langle \omega_D^p(R_0) \rangle \sim R_0^{-\chi_p^D}. \quad (9)$$

As we have discussed already, the multifractal model for incompressible turbulence does not distinguish between them [28–30] so the naive expectation is $\chi_p^H = \chi_p^D = p - \zeta_p$. On the contrary, our DNS shows (within the error bars of Fig. (3)),

$$\chi_p^H = p - \zeta_p \quad \text{and} \quad \chi_p^D = 2p/3; \quad (10)$$

clearly, $\chi_p^H \neq \chi_p^D$. Our extension of the multifractal model predicts the correct exponents in the following manner. The scaling of the moments of ω_D and ω_H , for $p > 1$, is determined primarily by the small- τ_D and small- τ_H behaviors of their respective PDFs. The short-time growth of R_0 can occur only if the interval is away from the shocks [Case (3), but at short times]. Therefore, for all such intervals, $K \sim R^{4/3}$ and consequently $\chi_p^D = 2p/3$ for all p [dashed line in Fig. (3)], in agreement with the results of our DNS. As for χ_p^H , at short times, even for

incompressible turbulence, intervals can decrease, hence the prediction of the multifractal model holds.

In an earlier paper [65] we have investigated dynamic multiscaling in the 1D stochastically forced Burgers equation by using a slightly different formulation than we have used here. Instead of halving times, we have considered interval-collapse times, i.e., the time it takes for a Lagrangian interval to shrink to a point. We have shown that, in 1D, the interval-collapse-time PDF has power-law tails. In contrast, we now find that, in 2D, the PDF of halving times has exponential tails. In both 1D and 2D cases, the shocks play a key role in determining the multiscaling properties.

In summary, we have shown how to generalize the multifractal model for incompressible-fluid turbulence to the stochastically forced 2D Burgers equation, which is rich enough to display the complexities of shock-dominated turbulence. Our DNS demonstrates clearly that the statistics of halving times deviate starkly from those of doubling times. By generalizing the standard argument that is used to derive Richardson’s law from K41 theory, we have developed a theory that leads to a natural way of understanding the statistics of halving and doubling times. The key idea in this theory is that, when we consider a Lagrangian interval of length R , we must distinguish between Cases (1)-(3). Our theoretical arguments can be generalized to shock-dominated compressible turbulence, if the equal-time exponents ζ_p are known.

We expect shock-dominated turbulence in astrophysical systems at both high Mach and Reynolds numbers, e.g., in the interstellar media and molecular clouds, where the turbulence is driven by supernovae explosions. The dynamics of Lagrangian intervals in such flows provides useful insights into transport and mixing in these systems, which influence chemical kinetics and the rates of formation of stars and planetesimals [36]. We expect our generalization of Richardson’s law to apply to such systems. For compressible turbulence, where the irrotational and solenoidal components of the flow have similar energies, our theory may require further generalization. Our work brings out the importance of calculating the statistics of both halving and doubling times of Lagrangian intervals from DNSs of compressible turbulent flows, for trans-sonic, super-sonic, and hyper-sonic cases.

ACKNOWLEDGMENTS

DM acknowledges the financial support of the Swedish Research Council through grants 638-2013-9243 and 2016-05225. NORDITA is partially supported by Nord-Forsk. SD thanks the PMRF (India) for support. RP and SD thank the Science and Engineering Research Board (SERB) and the National Supercomputing Mission (NSM), India for support, and the Supercomputer Education and Research Centre (IISc) for computational resources.

- [1] William R. Young, “Stirring and mixing,” in *Summer Program in Geophysical Fluid Dynamics, 1999*, edited by J-L Thiffeault and C Pasquero (1999).
- [2] G. Falkovich, K. Gawędzki, and M. Vergassola, *Rev. Mod. Phys.* **73**, 913 (2001).
- [3] G. K. Batchelor, “Diffusion in a field of homogeneous turbulence: II. the relative motion of particles,” *Mathematical Proceedings of the Cambridge Philosophical Society* **48**, 345–362 (1952).
- [4] Brian Sawford, “Turbulent relative dispersion,” *Annual Review of Fluid Mechanics* **33**, 289–317 (2001), <https://doi.org/10.1146/annurev.fluid.33.1.289>.
- [5] Juan P.L.C. Salazar and Lance R. Collins, “Two-particle dispersion in isotropic turbulent flows,” *Annual Review of Fluid Mechanics* **41**, 405–432 (2009), <https://doi.org/10.1146/annurev.fluid.40.111406.102224>.
- [6] Matthew Huber, James C. McWilliams, and Michael Ghil, “A climatology of turbulent dispersion in the troposphere,” *Journal of the Atmospheric Sciences* **58**, 2377–2394 (2001).
- [7] S. Edouard, B. Legras, F. Lefèvre, and R. Eymard, “The effect of small-scale inhomogeneities on ozone depletion in the arctic,” *Nature* **384**, 444–447 (1996).
- [8] Annalisa Griffa, Angélique Haza, Tamay M. Özgökmen, Anne Molcard, Vincent Taillandier, Katrin Schroeder, Yeon Chang, and P.-M. Poulain, “Investigating transport pathways in the ocean,” *Deep Sea Research Part II: Topical Studies in Oceanography* **85**, 81–95 (2013), *modern Physical Oceanography and Professor H.T. Rossby*.
- [9] Roberto Benzi and Federico Toschi, “Lectures on turbulence,” *Physics Reports* **1021**, 1–106 (2023).
- [10] Lewis Fry Richardson and Gilbert Thomas Walker, “Atmospheric diffusion shown on a distance-neighbour graph,” *Proceedings of the Royal Society of London. Series A, Containing Papers of a Mathematical and Physical Character* **110**, 709–737 (1926).
- [11] U. Frisch, *Turbulence: the legacy of A.N. Kolmogorov* (Cambridge University Press, Cambridge, 1996).
- [12] The angular brackets denote the average over the turbulent, but statistically steady, state of the fluid; and the length scale ℓ lies between the large length L_I , at which energy is injected, and the small length scale η , at which viscous dissipation becomes significant.
- [13] V.S. L’vov, E. Podivilov, and I. Procaccia, *Phys. Rev. E* **55**, 7030 (1997).
- [14] D. Mitra and R. Pandit, “Dynamic multiscaling in fluid turbulence: an overview,” *Physica A* **318**, 179 (2003).
- [15] D. Mitra and R. Pandit, “Varieties of dynamic multiscaling in fluid turbulence,” *Phys. Rev. Lett.* **93**, 024501 (2004).
- [16] S.S. Ray, D. Mitra, and R. Pandit, “The universality of dynamic multiscaling in homogeneous, isotropic navier-stokes and passive-scalar turbulence.” *New. J. Phys* **10**, 033003 (2008).
- [17] Samriddhi Sankar Ray, Dhruvaditya Mitra, Prasad Perlekar, and Rahul Pandit, “Dynamic multiscaling in two-dimensional fluid turbulence,” *Phys. Rev. Lett.* **107**, 184503 (2011).
- [18] Søren Ott and Jakob Mann, “An experimental investigation of the relative diffusion of particle pairs in three-dimensional turbulent flow,” *Journal of Fluid Mechanics* **422**, 207–223 (2000).
- [19] Ron Shnapp, Alex Liberzon, et al., “Generalization of turbulent pair dispersion to large initial separations,” *Physical Review Letters* **120**, 244502 (2018).
- [20] GE Elsinga, T Ishihara, and JCR Hunt, “Non-local dispersion and the reassessment of richardson’s t3-scaling law,” *Journal of Fluid Mechanics* **932**, A17 (2022).
- [21] Shiyong Tan and Rui Ni, “Universality and intermittency of pair dispersion in turbulence,” *Phys. Rev. Lett.* **128**, 114502 (2022).
- [22] Ron Shnapp, Stefano Brizzolara, Marius M Neamtu-Halic, Alessandro Gambino, and Markus Holzner, “Universal alignment in turbulent pair dispersion,” *Nature Communications* **14**, 4195 (2023).
- [23] Juan PLC Salazar and Lance R Collins, “Two-particle dispersion in isotropic turbulent flows,” *Annual review of fluid mechanics* **41**, 405–432 (2009).
- [24] Rehab Bitane, Holger Homann, and Jérémie Bec, “Time scales of turbulent relative dispersion,” *Physical Review E* **86**, 045302 (2012).
- [25] Rehab Bitane, Holger Homann, and Jérémie Bec, “Geometry and violent events in turbulent pair dispersion,” *Journal of Turbulence* **14**, 23–45 (2013).
- [26] Andrew D Bragg, Peter J Ireland, and Lance R Collins, “Forward and backward in time dispersion of fluid and inertial particles in isotropic turbulence,” *Physics of Fluids* **28** (2016).
- [27] Dhawal Buaria, Brian L Sawford, and Pui-Kuen Yeung, “Characteristics of backward and forward two-particle relative dispersion in turbulence at different reynolds numbers,” *Physics of Fluids* **27** (2015).
- [28] G. Boffetta and I. M. Sokolov, “Relative dispersion in fully developed turbulence: The richardson’s law and intermittency corrections,” *Phys. Rev. Lett.* **88**, 094501 (2002).
- [29] G. Boffetta and I. M. Sokolov, “Statistics of two-particle dispersion in two-dimensional turbulence,” *Physics of Fluids* **14**, 3224–3232 (2002).
- [30] G. Boffetta, A. Celani, A. Crisanti, and A. Vulpiani, “Pair dispersion in synthetic fully developed turbulence,” *Phys. Rev. E* **60**, 6734–6741 (1999).
- [31] V. Artale, G. Boffetta, A. Celani, M. Cencini, and A. Vulpiani, “Dispersion of passive tracers in closed basins: Beyond the diffusion coefficient,” *Physics of Fluids* **9**, 3162–3171 (1997).
- [32] Roberto Benzi, Giovanni Paladin, Giorgio Parisi, and Angelo Vulpiani, “On the multifractal nature of fully developed turbulence and chaotic systems,” *Journal of Physics A: Mathematical and General* **17**, 3521 (1984).
- [33] Giorgio Parisi and Uriel Frisch, “On the singularity structure of fully developed turbulence,” *Turbulence and predictability in geophysical fluid dynamics and climate dynamics*, Varenna, 1983, M. Ghil, R. Benzi and G. Parisi, eds. *Proceedings of the International School of Physics Enrico Fermi, North-Holland 1985*, 84–88 (1985).
- [34] U. Frisch, *Turbulence: The Legacy of A.N. Kolmogorov* (Cambridge University Press, Cambridge, England, 1996).
- [35] Hideaki Miura, “Enstrophy generation in a shock-dominated turbulence,” *Journal of the Physical Society of Japan* **65**, 450–461 (1996).

- [36] Mordecai-Mark Mac Low and Ralf S. Klessen, “Control of star formation by supersonic turbulence,” *Rev. Mod. Phys.* **76**, 125–194 (2004).
- [37] Wolfram Schmidt, Christoph Federrath, and Ralf Klessen, “Is the scaling of supersonic turbulence universal?” *Phys. Rev. Lett.* **101**, 194505 (2008).
- [38] Lukas Konstandin, Christoph Federrath, Ralf S. Klessen, and Wolfram Schmidt, “Statistical properties of supersonic turbulence in the Lagrangian and Eulerian frameworks,” *J. Fluid Mech.* **692**, 183 (2012).
- [39] Jianchun Wang, Yantao Yang, Yipeng Shi, Zuoli Xiao, XT He, and Shiyi Chen, “Cascade of kinetic energy in three-dimensional compressible turbulence,” *Physical review letters* **110**, 214505 (2013).
- [40] Jianchun Wang, Yantao Yang, Yipeng Shi, Zuoli Xiao, XT He, and Shiyi Chen, “Statistics and structures of pressure and density in compressible isotropic turbulence,” *Journal of Turbulence* **14**, 21–37 (2013).
- [41] Shriram Jagannathan and Diego A Donzis, “Reynolds and mach number scaling in solenoidally-forced compressible turbulence using high-resolution direct numerical simulations,” *Journal of Fluid Mechanics* **789**, 669–707 (2016).
- [42] Jianchun Wang, Toshiyuki Gotoh, and Takeshi Watanabe, “Spectra and statistics in compressible isotropic turbulence,” *Physical Review Fluids* **2**, 013403 (2017).
- [43] Diego A Donzis and John Panickacheril John, “Universality and scaling in homogeneous compressible turbulence,” *Physical Review Fluids* **5**, 084609 (2020).
- [44] Yoshiki Sakurai and Takashi Ishihara, “Direct numerical simulations of compressible isothermal turbulence in a periodic box: Reynolds number and resolution-level dependence,” *Physical Review Fluids* **8**, 084606 (2023).
- [45] Yantao Yang, Jianchun Wang, Yipeng Shi, Zuoli Xiao, X. T. He, and Shiyi Chen, “Intermittency caused by compressibility: A Lagrangian study,” *J. Fluid Mech.* **786**, R6 (2016).
- [46] Zhenhua Xia, Yipeng Shi, Qingqing Zhang, and Shiyi Chen, “Modulation to compressible homogenous turbulence by heavy point particles. I. Effect of particles’ density,” *Phys. Fluids* **28**, 016103 (2016).
- [47] J. R. Cressman, W. I. Goldburg, and J. Schumacher, “Dispersion of tracer particles in a compressible flow,” *Europhysics Letters* **66**, 219 (2004).
- [48] J. R. Cressman and W. I. Goldburg, “Compressible flow: Turbulence at the surface,” *J. Stat. Phys.* **113**, 875 (2003).
- [49] John R Cressman, Jahanshah Davoudi, Walter I Goldburg, and Jörg Schumacher, “Eulerian and lagrangian studies in surface flow turbulence,” *New Journal of Physics* **6**, 53 (2004).
- [50] Sébastien Galtier and Supratik Banerjee, “Exact relation for correlation functions in compressible isothermal turbulence,” *Phys. Rev. Lett.* **107**, 134501 (2011).
- [51] C. Federrath, “On the universality of supersonic turbulence,” *Monthly Notices of the Royal Astronomical Society* **436**, 1245–1257 (2013).
- [52] A. L. Barabási and H. E. Stanley, *Fractal Concepts in Surface Growth* (Cambridge University Press, 1995).
- [53] J. M. Burgers, “A Mathematical Model Illustrating the Theory of Turbulence,” (Elsevier, 1948) pp. 171–199.
- [54] Uriel Frisch and Jérémie Bec, “Burgulence,” in *New trends in turbulence Turbulence: nouveaux aspects* (Springer, 2001) pp. 341–383.
- [55] J. Bec, U. Frisch, and K. Khanin, “Kicked Burgers turbulence,” *J. Fluid Mech.* **416**, 239–267 (2000).
- [56] J. Bec and K. Khanin, “Burgers Turbulence,” *Phys. Rep.* **447**, 1–66 (2007).
- [57] Jérémie Bec, “Universality of Velocity Gradients in Forced Burgers Turbulence,” *Phys. Rev. Lett.* **87**, 104501 (2001).
- [58] A. M. Polyakov, “Turbulence without pressure,” *Phys. Rev. E* **52**, 6183–6188 (1995).
- [59] Ernesto Medina, Terence Hwa, Mehran Kardar, and Yi-Cheng Zhang, “Burgers equation with correlated noise: Renormalization-group analysis and applications to directed polymers and interface growth,” *Phys. Rev. A* **39**, 3053–3075 (1989).
- [60] Alexei Chekhlov and Victor Yakhot, “Kolmogorov turbulence in a random-force-driven Burgers equation,” *Phys. Rev. E* **51**, R2739–R2742 (1995).
- [61] F. Hayot and C. Jayaprakash, “Structure functions in the stochastic Burgers equation,” *Phys. Rev. E* **56**, 227–230 (1997).
- [62] F. Hayot and C. Jayaprakash, “Multifractality in the stochastic Burgers equation,” *Phys. Rev. E* **54**, 4681–4684 (1996).
- [63] F. Hayot and C. Jayaprakash, “From scaling to multiscaling in the stochastic Burgers equation,” *Phys. Rev. E* **56**, 4259–4262 (1997).
- [64] Dhruvadya Mitra, Jérémie Bec, Rahul Pandit, and Uriel Frisch, “Is Multiscaling an Artifact in the Stochastically Forced Burgers Equation?” *Phys. Rev. Lett.* **94**, 194501 (2005).
- [65] S. De, D. Mitra, and R. Pandit, “Dynamic multiscaling in stochastically forced burgers turbulence,” *Sci. Rep.* **13**, 7151 (2023).
- [66] Alexei Chekhlov and Victor Yakhot, “Kolmogorov turbulence in a random-force-driven burgers equation: Anomalous scaling and probability density functions,” *Phys. Rev. E* **52**, 5681–5684 (1995).
- [67] The numerical values of ζ_p , measured from our DNS, deviate slightly from (3) for $p \gtrsim 3$ (see Appendix A), possibly because of certain numerical artifacts identified in an earlier similar study in one dimension [64]. Whether this deviation is a numerical artefact or not in 2D is not our main focus here.
- [68] B. Castaing, Y. Gagne, and E.J. Hopfinger, “Velocity probability density functions of high reynolds number turbulence,” *Physica D: Nonlinear Phenomena* **46**, 177–200 (1990).
- [69] S. Y. Chen, B. Dhruva, S. Kurien, K. R. Sreenivasan, and M. A. Taylor, “Anomalous scaling of low-order structure functions of turbulent velocity,” *Journal of Fluid Mechanics* **533**, 183–192 (2005).
- [70] An alternative argument is as follows. By K41-type arguments, the only two quantities than can appear in constructing K are ε and R , where ε is the energy dissipation rate per unit mass. Hence $K \sim \varepsilon^{1/3} R^{4/3}$.
- [71] Sidney Redner, *A guide to first-passage processes* (Cambridge university press, 2001).
- [72] R.S. Rogallo, “Numerical experiments in homogeneous turbulence,” *NASA Technical Report* , 1–91 (1972).
- [73] C. Canuto, M.Y. Hussaini, A. Quarteroni, and T.A. Zang, *Spectral methods in Fluid Dynamics* (Spinger-Verlag, Berlin, 1988).

- [74] S.M. Cox and P.C. Matthews, “Exponential time differencing for stiff systems,” *Journal of Computational Physics* **176**, 430–455 (2002).
- [75] D.J. Higham, “An algorithmic introduction to numerical simulations of stochastic differential equations.” *SIAM Review* **43**, 525–546 (2001).
- [76] Anirban Sain, Manu, and Rahul Pandit, “Turbulence and multiscaling in the randomly forced navier-stokes equation,” *Phys. Rev. Lett.* **81**, 4377–4380 (1998).
- [77] P.K. Yeung and S.B. Pope, *J. Fluid Mech.* **207**, 531 (1989).

Appendix A: Direct Numerical Simulations

We perform pseudospectral direct numerical simulations (DNSs) of the randomly forced 2D Burgers equation

$$\begin{aligned} \partial_t \mathbf{u} + \mathbf{u} \cdot \nabla \mathbf{u} &= \nu \nabla^2 \mathbf{u} + \mathbf{f}(\mathbf{x}, t); \quad \nabla \times \mathbf{u} = 0; \\ \langle \hat{\mathbf{f}}(\mathbf{k}, t) \cdot \hat{\mathbf{f}}(\mathbf{k}', t') \rangle &\sim |\mathbf{k}|^{-2} \delta(\mathbf{k} + \mathbf{k}') \delta(t - t'); \end{aligned} \quad (\text{A1})$$

on a square, doubly-periodic domain of side length $L = 2\pi$ and with N^2 collocation points. We use the 2/3-dealiasing [72, 73] scheme to remove aliasing errors and the second-order exponential time-differencing Runge-Kutta (ETDRK2) scheme [74] for the time evolution of the velocity field. The stochastic force is incorporated by using the Euler-Maruyama scheme [75]. The parameters of our DNS runs are given in Table I.

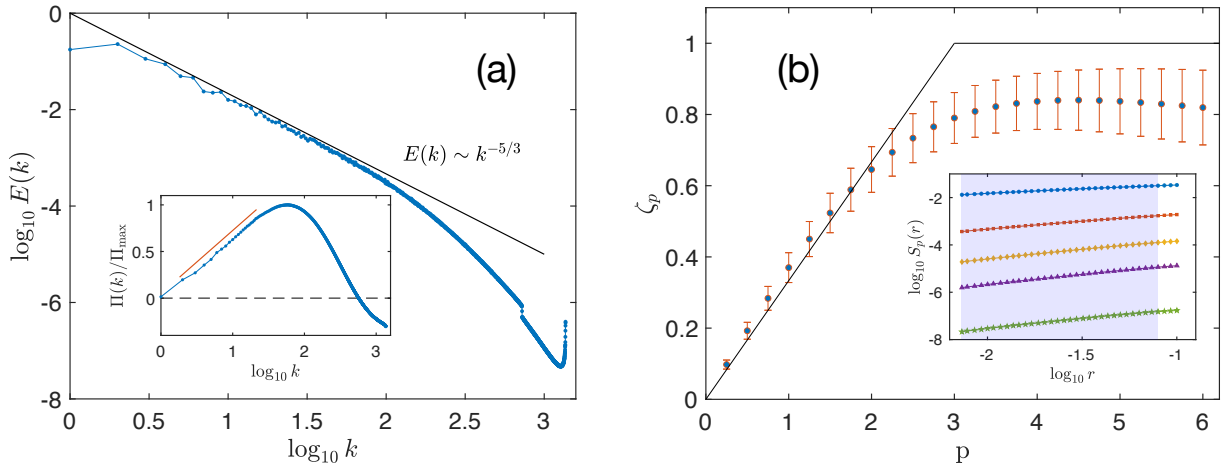


FIG. 4. (a) Log-log plot versus the wave number k of the energy spectrum $E(k)$ (averaged over shells of radius k in Fourier space and over time in the nonequilibrium statistically steady turbulent state); the inertial range extends over nearly a decade and a half in k , with $E(k) \sim k^{-5/3}$ (black line). *Inset*: Net energy flux $\Pi(k)$ through the wave-number scale k , displaying a direct cascade of energy; the red straight line indicates $\Pi(k) \sim A \log k$, where A is a constant, as suggested on theoretical grounds for the randomly-forced 1D Burgers and 3D randomly forced Navier-Stokes turbulence [64, 76]. (b) Equal-time structure function exponents, ζ_p , versus p ; the black lines represent bifractal scaling. *Inset*: Log-log plots of the Eulerian equal-time structure functions, $S_p(r)$, versus r for $p = 1$ (circles), $p = 2$ (squares), $p = 3$ (triangles), $p = 4$ (triangles) and $p = 6$ (stars); the shaded region denotes the regime of best power-law fit within the inertial regime; ζ_p are calculated via local slope analyses of these curves.

N	ν	δt	\mathcal{L}_I	u_{rms}	Re	η	T_L	$k_{\text{max}} \eta$
4096	5×10^{-5}	5×10^{-4}	0.25	0.05	1.61×10^3	5.6×10^{-3}	30.0	7.7

TABLE I. Parameters for our direct numerical simulations (DNS): N is the number of collocation points, ν the kinematic viscosity, δt the time step, $\mathcal{L}_I \equiv \frac{3\pi}{4} \frac{\int \frac{E(k)}{k} dk}{\int E(k) dk}$ the integral length scale (normalized by 2π here), u_{rms} the root-mean-square velocity, $\text{Re} = u_{\text{rms}} \mathcal{L}_I / \nu$ the integral-scale Reynolds number, $\eta \equiv \left(\frac{\nu^3}{\epsilon}\right)^{1/4}$ the dissipation length scale, where ϵ is the mean energy dissipation rate, $T_L \equiv \mathcal{L}_I / u_{\text{rms}}$ the large-eddy-turnover time, and k_{max} the de-aliasing cutoff.

Figure 4(a) displays the ensemble-averaged energy spectrum,

$$E(k) \equiv \frac{1}{2} \sum_{|\mathbf{k}|=k} |\hat{\mathbf{u}}(\mathbf{k})|^2, \quad (\text{A2})$$

in the non-equilibrium statistically steady state (NESS). In the inertial range, the power-law behavior of the energy spectrum is consistent with $E(k) \sim k^{-5/3}$ over more than a decade and half [64, 65] in wavenumber k . The scale-to-scale energy flux, $\Pi(k)$, through the scale k is not constant in the inertial range but has logarithmic corrections, i.e., $\Pi(k) \sim \log k$, which is agreement with earlier results in randomly forced turbulence wherein all modes up to a cut-off, $k_c \gg k$ (with k in the inertial range), are forced randomly [see Refs. [64, 76] for details]; we choose $k_c = \sqrt{2}N/8$. We calculate the longitudinal equal-time structure functions,

$$S_p(r) = \langle |\delta \mathbf{u}(\mathbf{r}) \cdot \hat{r}|^p \rangle \sim r^{\zeta_p}, \quad \text{where} \quad (\text{A3a})$$

$$\delta \mathbf{u}(\mathbf{r}) = \mathbf{u}(\mathbf{x} + \mathbf{r}) - \mathbf{u}(\mathbf{x}). \quad (\text{A3b})$$

Here \hat{r} is the unit vector in the direction of \mathbf{r} . We plot $S_p(r)$ in the inset of Fig. (4b) on a log-log graph; in the inertial range, $\eta/L \ll r \ll 1$, we find clean power-law scaling for $S_p(r)$; by carrying out local slope analyses, we evaluate the exponents ζ_p that we show in Fig. (4b). These exponents are close to the bifractal scaling predicted for stochastically forced 1D Burgers turbulence [64, 66]; whether their deviation from the bifractal prediction for $p \geq 3$ signifies bonafide multiscaling (or is simply a numerical artifact) requires in-depth theoretical and numerical analysis, both of which lie beyond the scope of this article.

The equation of motion of a Lagrangian particle or tracer is

$$\frac{d}{dt} \mathbf{X}(t) = \mathbf{u}(\mathbf{X}, t), \quad (\text{A4})$$

where $\mathbf{X}(t)$ is the position of the tracer at time t . After the flow has reached the NESS, we seed the flow uniformly with $N_p = 2048^2$ tracers on a square grid; subsequently, we track their motion by solving (A4), where we calculate $\mathbf{u}(\mathbf{X}, t)$ via bilinear interpolation of the Eulerian velocities [77] to off-grid points.

Appendix B: Theory for halving time of Lagrangian intervals

We now outline the steps that are necessary to model the pair diffusivity $K(R)$ of a Lagrangian interval of size R . Once we have $K(R)$ we derive, from the corresponding Fokker-Planck equations, the asymptotic forms of the PDFs of the halving times of the Lagrangian intervals with initial size R_0 , that lies in the inertial range [see Eq. (6) in the main text].

The velocity difference $\delta_R V$, across an interval of length R , is either

1. a constant independent of R , when the interval straddles a shock,
2. or $\delta_R V \sim R^h$, where h is the local Hölder exponent of the velocity field; for the type of forcing we use, $h = 1/3$ [see e.g., 60, 66].

For a Lagrangian interval one of the following three cases must hold:

1. Case (1): the interval lies along a shock.
2. Case (2): the interval straddles a shock.
3. Case (3): the interval lies away from any shock.

There is the additional possibility that the two ends of the interval are in two different shocks. We show later that it is not necessary to consider this case separately.

Case (1) [see Fig. (5)]: Then the velocities at A and B are $(\mathbf{u}_1 + \mathbf{u}_2)/2$ and $(\mathbf{u}_3 + \mathbf{u}_4)/2$, respectively. Hence,

$$\delta_R V = (\mathbf{u}_1 - \mathbf{u}_3) \cdot \hat{R} + (\mathbf{u}_2 - \mathbf{u}_4) \cdot \hat{R} \quad (\text{B1})$$

As both the velocity differences on the right-hand-side of (B1) scale as R^h , $\delta_R V \sim R^h$. Furthermore, because both the ends of the interval are on the same shock, the typical correlation time $t_{\text{cor}} \sim R$ because of the sweeping effect. Therefore, $K \sim R^{1+2h}$.

Case (2): $\delta_R V$ is a constant independent of R and $t_{\text{cor}} \sim R$. Consequently, $K \sim R$.

Case (3): the interval can decrease in the following two ways.

1. Case (3A): both ends of the interval get trapped, at a later time, in the same shock, so the arguments used in Case (1) apply; but, after the interval is trapped on the shock, $K \sim R^{2h+1}$ at late times.

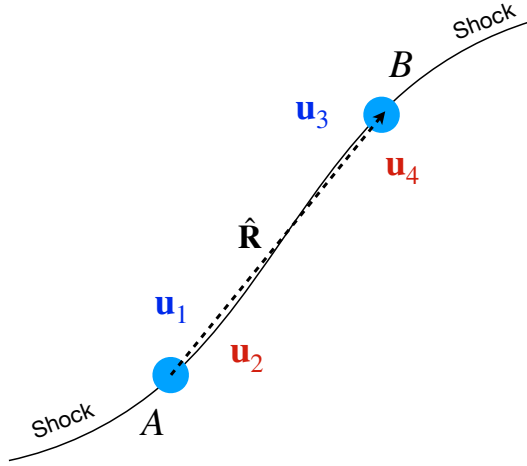


FIG. 5. Schematic diagram of a typical case of a Lagrangian interval of length R lying along a shock (solid line). A and B marks the two ends of the interval.

2. Case (3B): at late times the two ends of the interval get trapped in two different shocks which then approach each other. The velocity difference $\delta_R V$ is the velocity difference between two shocks; this does not depend on the distance between them, i.e., $\delta_R V$ is independent of R ; furthermore, $t_{\text{cor}} \sim R$, so $K \sim R$.

In all of these cases, the calculation of the PDF of halving times is a first-passage time problem for the following 2D Fokker-Planck equation for the the PDF $W(R, t)$ of R :

$$\partial_t W = \frac{1}{R} \partial_R [RK(R) \partial_R] W, \quad (\text{B2})$$

with absorbing boundaries at $R \rightarrow \infty$ and $R = R_0/2 \equiv R(t=0)/2$. It is sufficient to do such a calculation for the two cases with $K \sim R^{2h+1}$ and $K \sim R$. We make the change of variable $\xi = 1/R$, which maps the radial domain to the interval $[0, 2/R_0]$. The Fokker-Planck equation in ξ then reads,

$$\frac{\partial}{\partial t} W(\xi, t) = K_0 \xi^3 \frac{\partial}{\partial \xi} \left[\xi K(\xi) \frac{\partial}{\partial \xi} W(\xi, t) \right]. \quad (\text{B3})$$

We first consider the case $K \sim R^{1+2h}$, i.e., $K = K_0 \xi^{-1-2h}$, where K_0 is an R -independent constant. We define $y = \xi^{(2h-1)/2}$ and substitute it in (B3) to obtain

$$\frac{\partial}{\partial t} W(y, \tau) = K_0 \left(\frac{1-2h}{2} \right)^2 \left[\frac{\partial^2}{\partial y^2} + \left(\frac{3+2h}{1-2h} \right) \frac{1}{y} \frac{\partial}{\partial y} \right] W(y, t). \quad (\text{B4})$$

We solve (B4) with the boundary condition $W(y=Y, t) = 0$, where $Y = (2/R_0)^{(2h-1)/2}$, by separation of variables. We obtain

$$W(y, t) = \sum_n \frac{A_n}{y^q} J_q \left(\frac{c_n y}{Y} \right) \exp \left[-c_n^2 K_0 \left(\frac{1-2h}{2} \right)^2 \frac{t}{Y^2} \right], \quad (\text{B5})$$

where J_q is the order- q Bessel function of the first kind, where $q = (1+2h)/(1-2h)$, c_n is the n -th zero of J_q , and A_n is the normalization constant.

The initial distribution is $W(\xi, t=0) = W_0(\xi) = \delta(\xi - \xi_*)/2\pi\xi$, where $\xi_* = 1/R_0$. In the variable y we have

$$W_0(y) = \frac{1}{2\pi y^{2/(2h-1)}} \left(\frac{1-2h}{2} \right) (\sigma Y)^{(3-2h)/(1-2h)} \delta(y - \sigma Y), \quad (\text{B6})$$

where $\sigma = 1/2^{(2h-1)/2}$. We set $t=0$, multiply both sides of (B5) by $y^{q+1} J_q(c_m y/Y)$, integrate from $y=0$ to $y=Y\sigma$, and by using the orthogonality properties of Bessel functions, we get

$$A_m = \frac{1-2h}{4\pi} (\sigma Y)^{(5+2h)/(1-2h)} \frac{J_q(c_m/\sigma)}{J_{q+1}(c_m)}, \quad (\text{B7})$$

for any positive integer m . Thus,

$$W(y, t) = \frac{1-2h}{4\pi} (\sigma Y)^{(5+2h)/(1-2h)} \frac{1}{y^q} \sum_n \frac{J_q(c_n/\sigma)}{J_{q+1}(c_n)} J_q\left(\frac{c_n y}{Y}\right) \exp\left[-c_n^2 K_0 \left(\frac{1-2h}{2}\right)^2 \frac{t}{Y^2}\right]. \quad (\text{B8})$$

The survival probability is given by

$$\mathcal{S}(R_0, t) = \int_{\xi < 2/R_0} W(\xi, t) \xi d\xi d\theta. \quad (\text{B9})$$

In the new variable y , the area element $\xi d\xi d\theta = \frac{2}{1-2h} y^{(2h-5)/(1-2h)} dy d\theta$, so

$$\mathcal{S}(Y, t) = (\sigma Y)^{(5+2h)/(1-2h)} \sum_n \frac{J_q(c_n/\sigma)}{J_{q+1}(c_n)} \exp\left[-c_n^2 K_0 \left(\frac{1-2h}{2}\right)^2 \frac{t}{Y^2}\right] \int_0^Y y^{1+q} J_q\left(\frac{c_n y}{Y}\right) dy. \quad (\text{B10})$$

For large t , the $n = 1$ term dominates over the others. Hence, by retaining only its contribution and substituting $z = y/Y$ in the integrand, we get

$$\mathcal{S}(Y, t) \simeq G(\sigma) \exp\left[-c_1^2 K_0 \left(\frac{1-2h}{2}\right)^2 \frac{t}{Y^2}\right], \quad \text{where} \quad G(\sigma) = \sigma^{(5+2h)/(1-2h)} \frac{J_q(c_1/\sigma)}{J_{q+1}(c_1)} \int_0^1 z^{q+1} J_q(c_1 z) dz. \quad (\text{B11})$$

By replacing Y by $(2/R_0)^{(2h-1)/2}$, we can evaluate the halving-time distribution $\mathcal{P}_1(\tau_H, R_0)$ as follows:

$$\mathcal{P}_1(\tau_H, R_0) = -\frac{d}{d\tau} \mathcal{S}(R_0, \tau_H) \Big|_{t=\tau_H}, \quad (\text{B12})$$

whence we obtain the following asymptotic form:

$$\mathcal{P}_1(\tau_H, R_0) \sim \frac{1}{R_0^{1-2h}} \exp\left[-A_1 \frac{\tau_H}{R_0^{1-2h}}\right], \quad (\text{B13})$$

where A_1 is a numerical constant.

Similarly, for the intervals with $K \sim R$, we obtain the asymptotic form of their halving-time distribution:

$$\mathcal{P}_2(\tau_H, R_0) \sim \frac{1}{R_0} \exp\left[-A_2 \frac{\tau_H}{R_0}\right]. \quad (\text{B14})$$

For Cases (3A) and (3B), let τ_s be the time at which both ends of the interval get trapped on the same or different shocks, respectively. Then, for $\tau_H \gg \tau_s$, the halving-time distributions for Cases (3A) and (3B) reduce to \mathcal{P}_1 and \mathcal{P}_2 , respectively. Therefore, the overall halving-time PDF $\mathcal{P}(\tau_H, R_0)$, for an interval of initial size R_0 , is a weighted sum of all these cases [see Eq. (7) in the main text]. Thus, by retaining only the leading-order contribution in the limit $R_0 \ll 1$, we get

$$\mathcal{P}(\tau_H, R_0) \sim \mathcal{P}_1 \sim \frac{1}{R_0^{1-2h}} \exp\left[-A_1 \frac{\tau_H}{R_0^{1-2h}}\right], \quad (\text{B15})$$

which yields Eq. (8) in the main text.

To validate (B15), we evaluate the halving-time cumulative PDFs $Q(\tau_H)$ from our DNS, for different initial interval sizes R_0 , by using the rank-order method, which ensures that the CPDFs are free of binning errors. According to (B15) this CPDF scales as

$$Q(\tau_H, R_0) \sim \exp\left[-A_1 \frac{\tau_H}{R_0^{1-2h}}\right] \sim \exp\left[-A_1 \frac{\tau_H}{R_0^{1-2h}}\right]. \quad (\text{B16})$$

In Fig. (6), we plot $Q(\tau_H)$, for different values of R_0 in the inertial range, on a semilog graph. All the plots are consistent with exponential tails, which collapse onto a single line (shown dashed in the figure) on rescaling τ_H by R_0^{1-2h} ; this confirms our theoretical result.

Furthermore, to verify the assumption that $\tau_H \gg \tau_s$ for intervals belonging to Cases (3A) and (3B), we evaluate the following numerically:

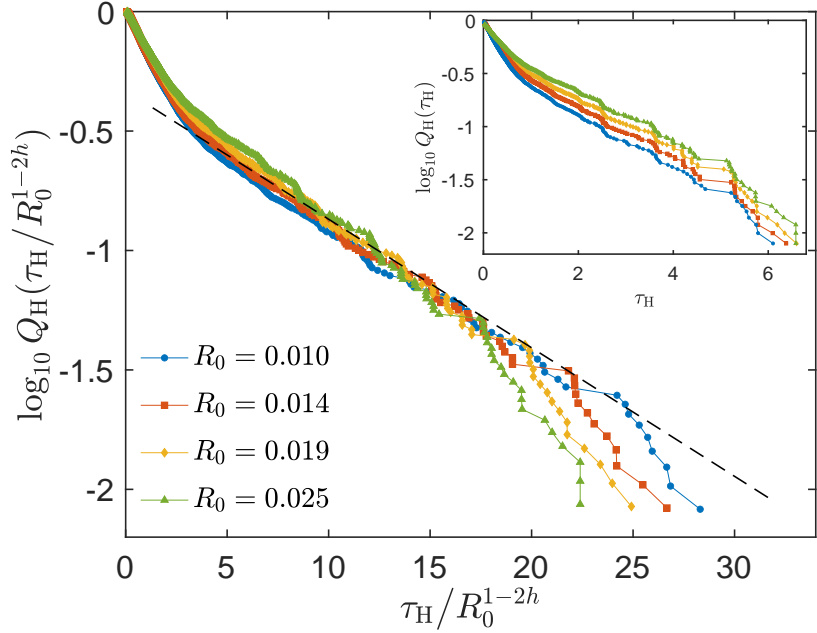


FIG. 6. **Cumulative PDF of halving times** The inset shows the semi-log plots of the cumulative PDFs (CPDFs) $Q(\tau_H)$ of halving times. The main figure shows the collapse of the PDFs, after τ_H is scaled by R_0^{1-2h} (see text for our theoretical result). The dashed straight line is drawn for reference. The main figure and the inset use the same colors and symbols.

1. The halving-time PDFs $\mathcal{P}_{\Lambda,H}$, of intervals whose lengths initially exceed a fixed threshold, $\Lambda = 1.5R_0$, before contracting.
2. The PDFs $\mathcal{P}_{\Lambda,s}$, of τ_s for these intervals.

The intervals in Cases (3A) and (3B) lie in the smooth regions of the flow at $t = 0$, so, at short times, they grow; and, as they do so, their ends fall on shocks which eventually lead to their contraction. Therefore, $\mathcal{P}_{\Lambda,H}$ and $\mathcal{P}_{\Lambda,s}$ are representative PDFs of τ_H and τ_s , respectively, for these intervals. We define τ_* to be the time at which such an interval size exceeds Λ and plot $\mathcal{P}_{\Lambda,H}$ and $\mathcal{P}_{\Lambda,s}$ as functions of $\tau'_H = (\tau_H - \tau_*)/\tau_*$ and $\tau'_{s'} = (\tau_s - \tau_*)/\tau_*$, respectively, for different values of R , in Fig. (7a). We observe that the tails of $\mathcal{P}_{\Lambda,H}$ are much broader than those of $\mathcal{P}_{\Lambda,s}$ for every value of R_0 . This provides compelling evidence in favor of our assumption that, generally $\tau_H \gg \tau_s$, for intervals belonging to Cases (3A) and (3B). For the purpose of visualization, we plot some representative time series of sizes, $R(t)$, of these intervals, coloured by the respective means of the instantaneous velocity divergences at their ends in Fig. (7b).

In Fig. 8 we present plots of the dependence of the moments of halving and doubling times on the initial interval size; we also give plots of negative-order equal-time structure functions.

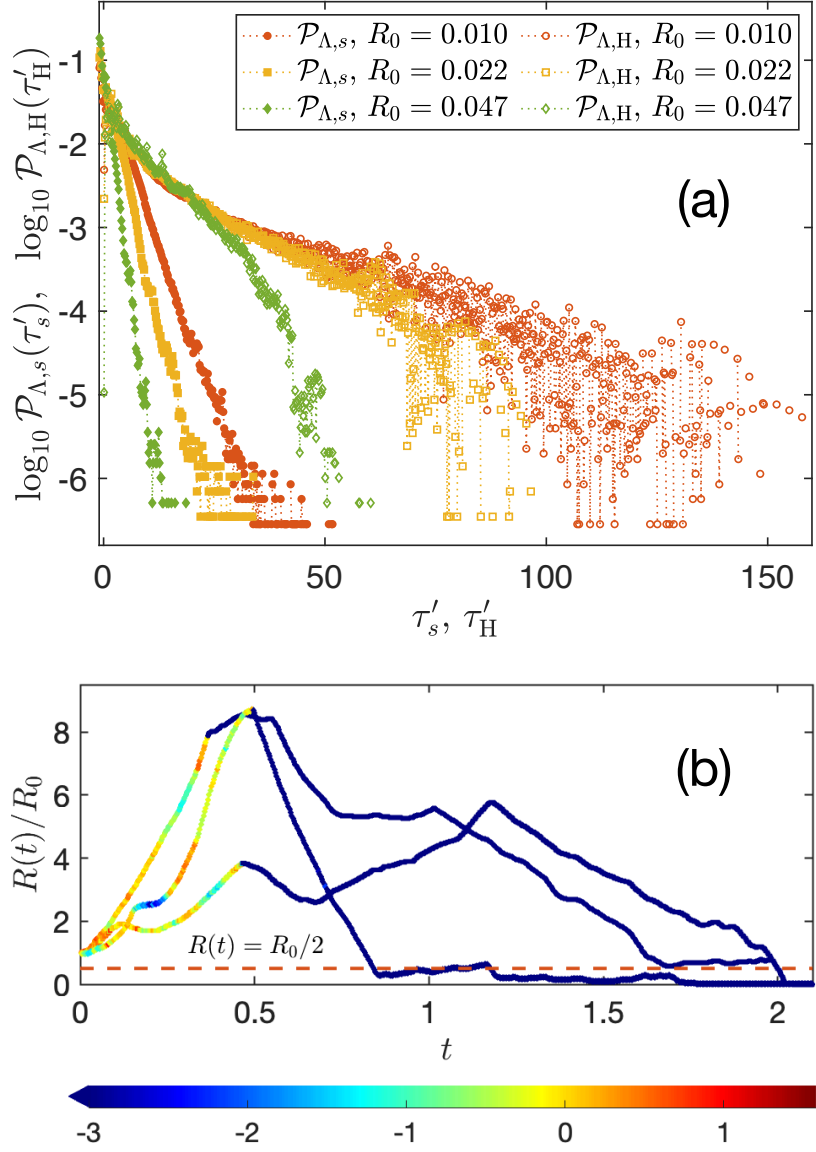


FIG. 7. (a) Semilog plots of $\mathcal{P}_{\Lambda,s}(\tau'_s)$ and $\mathcal{P}_{\Lambda,H}(\tau'_H)$ for different values of R_0 . This indicates that τ_H is generally much greater than τ_s for a typical interval belonging to Cases (3A) or (3B), for any R_0 . (b) Representative time series of interval sizes, $R(t)$, for $R_0 = 0.01$; colors denote the mean of the values of $\nabla \cdot \mathbf{u}$ at the two ends of the interval $R(t)$.

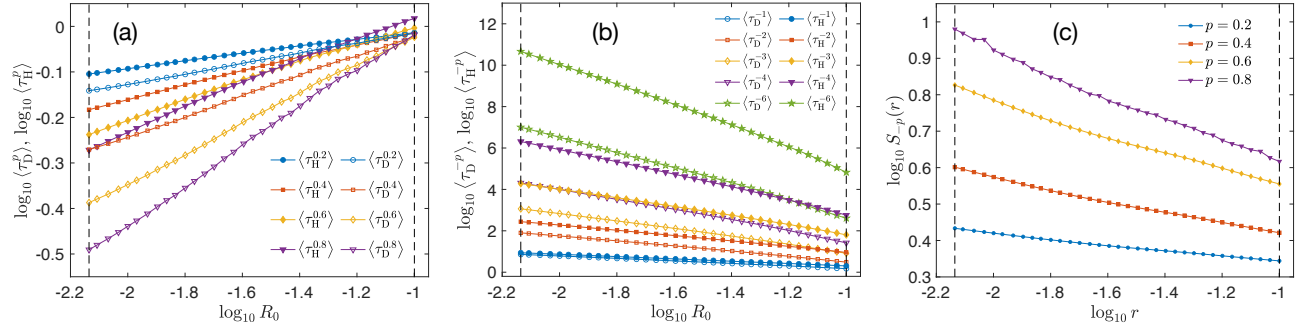


FIG. 8. Log-log plots of some of the (a) positive fractional moments (whose scaling exponents are shown in Fig. 2 in the main text) and (b) negative moments (whose scaling exponents are shown in Fig. 3 in the main text) of τ_H and τ_D as functions of the initial interval size R_0 . (c) Negative-order equal-time structure functions $S_{-p}(r)$ for different values of p ; the scaling exponents ζ_{-p} are also shown in Fig. 2 in the main text. In all these figures, the vertical lines indicate the boundaries of the regimes of local-slope analyses, which yield the various scaling exponents and their error bars. For all cases, the scaling regimes extend over more than a decade in the independent variable.